Elegant Approach for solving the Conservation Laws in Global Modelling of Radio-Frequency Ion Thrusters

IEPC-2019-A-612

Presented at the 36th International Electric Propulsion Conference
University of Vienna, Austria
September 15-20, 2019

Andreas Reeh* and U. Probst†
University of Applied Sciences, Giessen, Hessen, 35390, Germany

Peter J. Klar‡
University of Giessen, Giessen, Hessen, 35392, Germany

We present an overview of our simulation model for describing radio-frequency ion thrusters (RIT) including its peripheral components. The model is based on conservation equations for mass, charge and energy. For the plasma description a global modeling approach is used, where appropriate assumptions about the 6D phase space are made. To achieve more accurate results and to take into account the complex behaviour of the system, multiple numerical submodels such as an ion extraction code and an electromagnetic field solver are incorporated into the model. On the basis of our model we explain the difficulties to find the self-consistent solution of such a complex system of coupled equations. We define the term self-consistent solution and show that the mathematical problem of finding this solution can be considered a three-dimensional problem in the variable space spanned by the plasma parameters neutral gas density n_{n}, electron temperature T_{e}, and electron density n_{e} for fixed boundary conditions. We demonstrate that this problem can be reduced to a set of three 1D problems. For this purpose an appropriate structure of the underlying equation system is chosen with a suitable redefinition of the unknown variables and boundary conditions.

*Research Assistant and PhD student, Department of Electrical Engineering, andreas.reeh@ei.thm.de
†Professor, Department of Electrical Engineering, uwe.probst@ei.thm.de
‡Professor, Institute of Experimental Physics I, peter.j.klar@exp1.physik.uni-giessen.de

I. Introduction

RAdio-Frequency Ion Thrusters (RITs) as well as other gridded ion thrusters, are known for there relatively high specific impuls (I_{sp}) in the range of 3500 s to 6000 s and comparatively small divergence of the plume.[1] Feasible applications are north/south station keeping (inclination control) or orbit raising of telecommunication satellites. Furthermore, an utilization for deep space missions or formation flights is possible. Other than for Kaufman-type ion thrusters there is no need for heating electrodes inside the plasma. The underlying concept of a RIT is scalable over a nominal thrust range of many orders of magnitude.
For the optimization and development of such a complex system it is important to have appropriate models available. Based on these models simulations can be utilized to gain knowledge about the system's behaviour. This facilitates to derive optimization strategies. Furthermore, parameter studies can be simulated to optimize specific characteristics such as the geometry of thruster or the grids' apertures. Especial for such parameter studies short simulation times are important. Simulations may also give insight of parameters which are otherwise challenging to measure, such as the beamlets' ion density at the focus point between the grids.

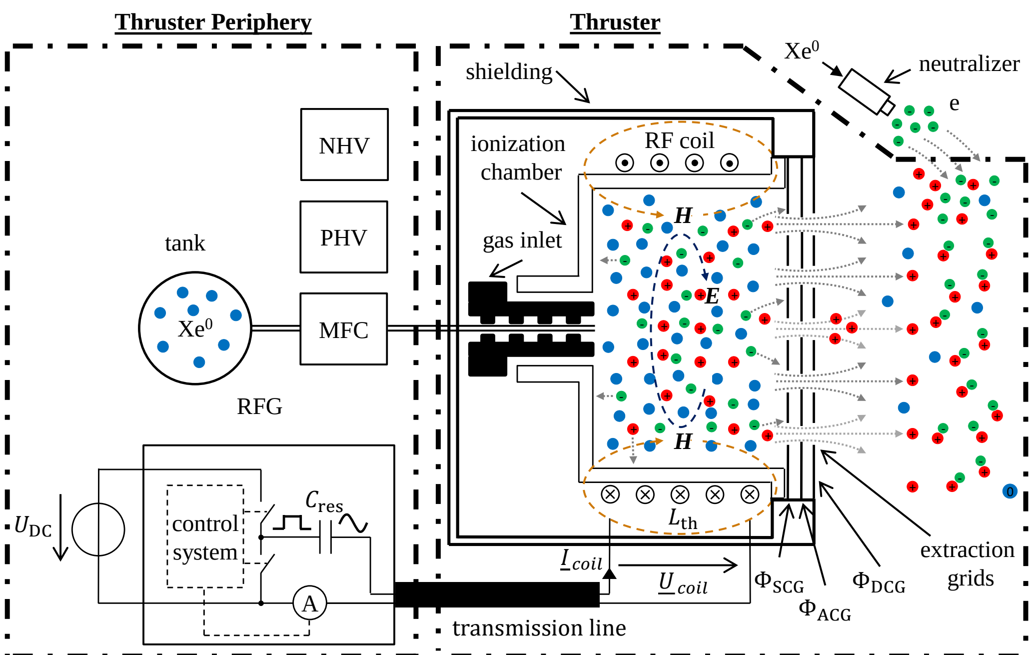

Figure 1. Operation principle of a RIT with its peripheral components

As depicted in Fig. 1 the thruster system can be divided in the peripheral components and the thruster itself. The periphery consists of a negative high voltage power supply (NHV), a positive high voltage power supply (PHV), a tank as propellant reservoir, a mass flow controller (MFC), the radio-frequency generator (RFG) and a transmission line. The thruster consists of a nonconductive ionization chamber, a gas inlet, the RF coil, a shielding surrounding the system and the extraction system. The latter consists typically of 2 grids with multiple aligned apertures. The analysis described in the following is based on the ion source "RIM-4" as depicted in Fig. 2 with 4 cm diameter of the ionization chamber is used. Its design is optimized for material processing and hence uses 3 grids.
An input mass flow $\dot{m}_{\mathrm{p}}$ will cause the neutral gas pressure inside the ionization chamber to rise. At a typical point of operation a regime of free molecular gas flow can be assumed where the amount of neutral particles lost via the grid system is nearly linear to the neutral gas pressure inside the ionization chamber. The pressure rises, until a steady state is reached where the mass flow $\dot{m}_{\mathrm{n,neutral}}$ of neutral particles lost through the grids equals $\dot{m}_{\mathrm{p}}$. The RFG used in this setup excites the electrical system with its series resonant frequency. The coil current generated by the RFG produces a magnetic field, which in turn induces a time-dependent electrical field inside the ionization chamber. After ignition of the plasma, this electrical field is used to

accelerate free electrons deterministically. As the electrons collide with neutrals, they scatter at random resulting in a heating of the plasma. Due to the electrostatic fields formed inside the low-pressure plasma, ions are accelerated towards the ionization vessel's walls. By applying grid voltages, an external electrostatic field is generated near the grids. Ions which move from the plasma towards the grids are accelerated by these external field to high velocity in the direction away from the thruster and, thus, produce the desired thrust. Due to the massflow of extracted ions, the neutral gas pressure will fall and a new steady state will be reached.

On the application level, i.e. for the satellite operator, the performance of the whole thruster system has to be considered. This also includes its peripheral components. Especially for the rf system, an optimization taking into account the whole thruster can be beneficial, as the losses both inside the RFG and the transmission line are strongly influenced by the thruster's design, especially its coil. For such optimizations the whole thruster system has to be simulated repeatedly. Therefore, it is advantageous and justified to employ a simplified plasma model based on global modeling, where assumptions are made with regard to the plasma' phase space rather than carrying out time-consuming microscopic calculations on single particle level for describing the plasma.

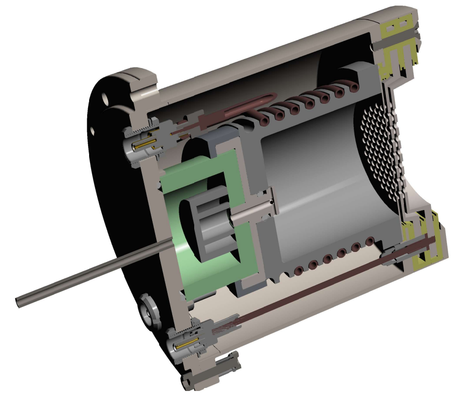

Figure 2. Geometry of the RIM-4

Furthermore, the model for the whole thruster system is based on conservation equations of mass, charge and energy yielding a set of rate equations. For each equation, i.e. state quantity, a balance of negative and positive contributing parts has to be achieved. Only in the simplest cases the individual contributing parts can be described analytically. For more realistic and accurate descriptions of the thruster the complexity increases and one has to numerically solve the problem. For this purpose the model is divided into submodels. This has been done in more recent works in Refs. 2–7. Consequently, the model is often seen as a set of interdependent individual numerical submodels rather than one system of equations. A flow chart to find the self-consistent solution based on the work presented in Ref. 7 is given in Fig. 3. For simplicity, individual submodels which are part of the conservation blocks are not shown. The algorithm starts with

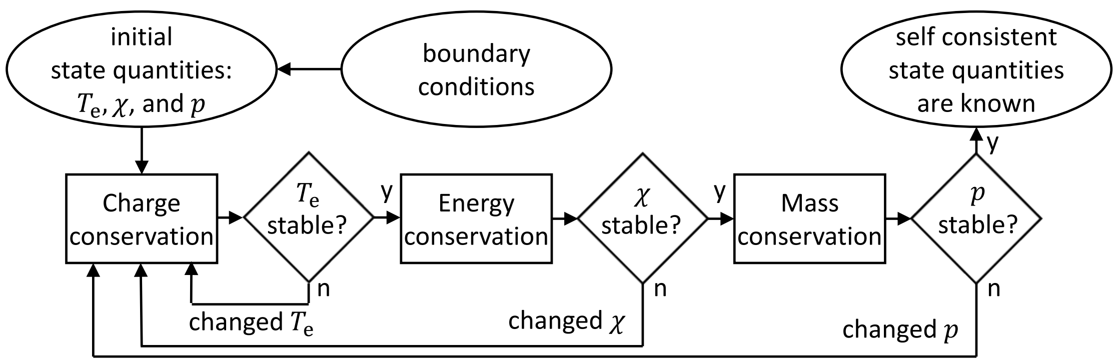

Figure 3. Flow chart for finding the self-consistent solution based on Ref. 7

initial values for the state quantities electron temperature T_e, ionisation degree χ and pressure p. These values are adjusted in an iterative manner until they have converged. The self-consistent solution is given by a set of values for the state quantities, that mathematically solve each submodule involved. Examples of such submodels are an ion optics code to consider non-linear behaviour due to direct impingement and crossover effects where ions impinge the grids, an electromagnetic field solver, a neutral gas simulation etc. An overview is given by Table 1. Due to the complexity of the model two challenges a) and b) arise:

a) Self-consistent solution
As illustrated in Fig. 3 the individual submodels are interconnected in a complex function, i.e. after being processed by other submodels, the output variable of one submodel will influence its own input variables. Thus, finding the self-consistent solution has a few obstacles:

1) The submodels are solved numerically, i.e. values for input variables have to be set and after the calculation values for the output variable/s are given. Therefore, a numerical algorithm has to be used to find the solution.

2) Using more complex submodels requires more computational power or calculation time. Consequently, the amount of necessary iterations for finding the self-consistent solution should by minimized.

3) The individual numerical submodels may be multidimensional, behave non-linearly and the output variables do not necessarily depend monotonically on the input variables. Consequently, finding a good estimate for the correction of the initial state variables, as desired in an iterative approach, gets complicated.

4) The algorithm used will find *one* solution, but does not necessarily yield information, whether the solution found is *unique*, i.e. there could be multiple solutions for the boundary conditions given.

b) Highly coupled system of equations

1) The example in Fig. 3 shows, that correcting the value of the state quantity p invalidates the former results for T_e and χ. The solution is given as the set of state quantities. Due to the interdependence of the submodules it is not possible to obtain just one state quantity without affecting the others. Consequently, if a specific submodel is changed in an optimization process the whole model has to be run to evaluate the influence of this change and to establish and verify consistency.

2) Emergent behaviour is formed due to the utilization of multiple interdependent submoduls. Furthermore, these submodels have complex characteristics as explained in a) 3. Consequently, the optimization of a single submodel more or less requires to simulate the whole system again. Without simulating the whole system it may be difficult to estimate, if the change made to a specific submodel improves or worsens the system's performance.

II. Elegant Approach for solving the Conservation Laws

A. Utilized submodels

An elegant approach to solve the system of interdependent submodules will be shown. To get a better understanding of the underlying system and the interdependence of the variables and submodels, all submodels are listed in Table 1. A specific submodel can be seen as a mathematical function which describes relationship between the output variable/s and the input variable/s. The submodels highlighted in red utilize some

Table 1. Overview of the submodels used

no.	state quantity	submodel	output variable/s	input variable
I	mass	conversion	$\dot{m}_\mathrm{n,i}$	I_b
II	mass	beam current model	I_b	n_es, T_e, τ_i, geometry
III	mass	ion extraction code	τ_i	n_es, T_e, Φ_SCG, Φ_ACG, Φ_DCG, geometry
IV	mass	neutral gas losses	$\dot{m}_\mathrm{n,neutral}$	τ_n, n_n, T_n
V	mass	neutral gas simulation	τ_n	geometry
VI	charge	generated current	I_p	n_e, n_n, T_e, cross sections, geometry
VII	charge	lost current	I_n	n_es, T_e, M, geometry
VIII	energy	power calculation	P_p	R_p, I_coil
IX	energy	EM field solver	R_p, $\underline{Z}_\mathrm{th}$	$\underline{\kappa}_\mathrm{p}$, T_m, geometry
X	energy	plasma conductivity model	$\underline{\kappa}_\mathrm{p}$	n_n, n_e, T_e, f, cross sections
XI	energy	plasma losses	P_n	n_e, n_n, T_e, M, n_es, cross sections, geometry
XII	energy	circuit model	I_coil, f	U_DC, R_p, L_th
XIII	multiple	electron density at sheath	n_es	n_e, n_n, σ_in, geometry

kind of iterative solving method and consequently a certain amount of computational power, respectively, computation time is necessary. In submodel I the massflow of lost ions $\dot{m}_{\mathrm{n,i}}$ can be calculated from the beam current I_{b}. In submodel II the value of I_{b} is calculated by the "beam current model" as a sum of multiple beamlet currents. For this purpose, the electron temperature T_{e} as one of the state variables, the electron density at the sheath position n_{es} from submodel XIII and the ion transmission coefficient τ_{i} calculated by submodel III are required. The latter variable is calculated by an "ion extraction code" where the grid voltages Φ_{SCG}, Φ_{ACG}, Φ_{DCG} are set. In submodel IV the mass flow of lost neutral particles $\dot{m}_{\mathrm{n,neutral}}$ is calculated as a sum of lost massflow per aperture pairing, with the neutral gas transmission coefficient τ_{n}, the neutral gas density inside the ionization vessel n_{n}, and the neutral gas temperatur T_{n}. Submodel V is used to calculate τ_{n} utilizing the test particle Monte-Carlo (TPMC) method. Submodels VI/VII define the charge conservation balance of current of generated ions I_{p} and current of lost ions I_{n}. For the calculation also the electron density inside the ionization chamber n_{e} and the gas particles mass M is needed. With the help of submodel VIII the power coupled into the plasma P_{p} can be calculated by the plasma resistance R_{p} and the coil current I_{coil}. In submodel XII the latter value could be determined by a circuit simulation (e.g. by utilization of a SPICE program) considering RFG and transmission line. Such a model would need the RFG's DC input voltage V_{DC}, R_{p} and the thruster's impedance $\underline{Z}_{\mathrm{th}}$ as input variable and provides I_{coil} as well as the excitation frequency f. As will be mentioned later, contrary to Table 1, we utilize a peripheral model with different characteristics. In submodels IX an electromagnetic field solver is used for simulating the thruster's impedance, which needs the plasma conductivity $\underline{\kappa}_{\mathrm{p}}$ given by submodel X and the material temperature T_{m} as input variables. Submodels XI/XIII provide the plasma losses P_{n} and n_{es} on the basis of macroscopic material parameters such as the cross section between ions and neutrals σ_{in}.

B. System of equations

All submodels introduced in Table 1 can be described mathematically as contributions to three balance equations. The system of equations for massflow $\Delta\dot{m} = 0$, generated ion current $\Delta I = 0$ and power $\Delta P = 0$ is shown in Eqs. 1, 2 and 3, respectively. Each balance equation is separated in its positive and negative contributions. The dependencies of these contributions on the variables is given in brackets

$$\Delta\dot{m}\left(\dot{m}_{\mathrm{p,neutral}}, T_{\mathrm{n}}, n_{\mathrm{n}}, T_{\mathrm{e}}, n_{\mathrm{e}}\right) = \dot{m}_{\mathrm{p,neutral}}\left(\right) - \dot{m}_{\mathrm{n}}\left(T_{\mathrm{n}}, n_{\mathrm{n}}, T_{\mathrm{e}}, n_{\mathrm{e}}\right) = 0 \tag{1}$$

$$\Delta I\left(n_{\mathrm{n}}, T_{\mathrm{e}}, n_{\mathrm{e}}\right) = I_{\mathrm{p}}\left(n_{\mathrm{n}}, T_{\mathrm{e}}, n_{\mathrm{e}}\right) - I_{\mathrm{n}}\left(n_{\mathrm{n}}, T_{\mathrm{e}}, n_{\mathrm{e}}\right) = 0 \tag{2}$$

$$\Delta P\left(U_{\mathrm{DC}}, T_{\mathrm{m}}, n_{\mathrm{n}}, T_{\mathrm{e}}, n_{\mathrm{e}}\right) = P_{\mathrm{p}}\left(U_{\mathrm{DC}}, T_{\mathrm{m}}, n_{\mathrm{n}}, T_{\mathrm{e}}, n_{\mathrm{e}}\right) - P_{\mathrm{n}}\left(n_{\mathrm{n}}, T_{\mathrm{e}}, n_{\mathrm{e}}\right) = 0 \tag{3}$$

where $\dot{m}_{\mathrm{p,neutral}}$ is the input mass flow of neutrals into the ionization chamber. The mass flow lost towards space $\dot{m}_{\mathrm{n}}\left(T_{\mathrm{n}}, n_{\mathrm{n}}, T_{\mathrm{e}}, n_{\mathrm{e}}\right)$ can be further divided into contributions

$$\dot{m}_{\mathrm{n}}\left(T_{\mathrm{n}}, n_{\mathrm{n_0}}, T_{\mathrm{e}}, n_{\mathrm{e}}\right) = \dot{m}_{\mathrm{n,i}}\left(T_{\mathrm{e}}, n_{\mathrm{e}}\right) + \dot{m}_{\mathrm{n,neutral}}\left(T_{\mathrm{n}}, n_{\mathrm{n}}\right). \tag{4}$$

The state quantities used by our model $n_{\mathrm{n}}, T_{\mathrm{e}}$, and n_{e} are marked in red colour to indicate that they are unknown, whereas the variables marked in blue colour $U_{\mathrm{DC}}, T_{\mathrm{n}}, T_{\mathrm{m}}$, and $\dot{m}_{\mathrm{p,neutral}}$ are known variables (boundary conditions). The system consists of three non-linear equations with seven unknown variables. To solve the system at least four variables must be defined as boundary conditions. In our case T_{n} and T_{m} will serve as boundary conditions as no temperature submodule is utilized. The most obvious choice of the other two boundary conditions would be the remaining external variables U_{DC} and $\dot{m}_{\mathrm{p,neutral}}$, which are also typically set in an experiment. The remaining task then is to solve the system for the plasma state quantities $n_{\mathrm{n}}, T_{\mathrm{e}}$, and n_{e}. Remaining variables, such as the beam current I_{b}, can be calculated from the resulting state quantities.

C. Visualization of the problem

Each balance equation has a set of possible solutions which correspond to a surface in a three-dimensional coordinate system spanned by the state quantities $n_{\mathrm{n}}, T_{\mathrm{e}}$, and n_{e}. Examples of such surfaces given by boundary conditions $\dot{m}_{\mathrm{p,neutral}} = 1.5$ sccm and $T_{\mathrm{n}} = T_{\mathrm{m}} = 150°\mathrm{C}$ are given in Fig. 4 for the mass and charge conservation. Each point of the surfaces shown represents a set of state quantities for which the corresponding balance equation is fulfilled. To explain Fig. 4 a), we rearrange the mass conservation and take advantage of the linear dependence between $\dot{m}_{\mathrm{n,i}}$ and I_{b} to formulate:

$$I_{\mathrm{b}} \propto \dot{m}_{\mathrm{n,i}} = \dot{m}_{\mathrm{p,neutral}} - \dot{m}_{\mathrm{n,neutral}} \tag{5}$$

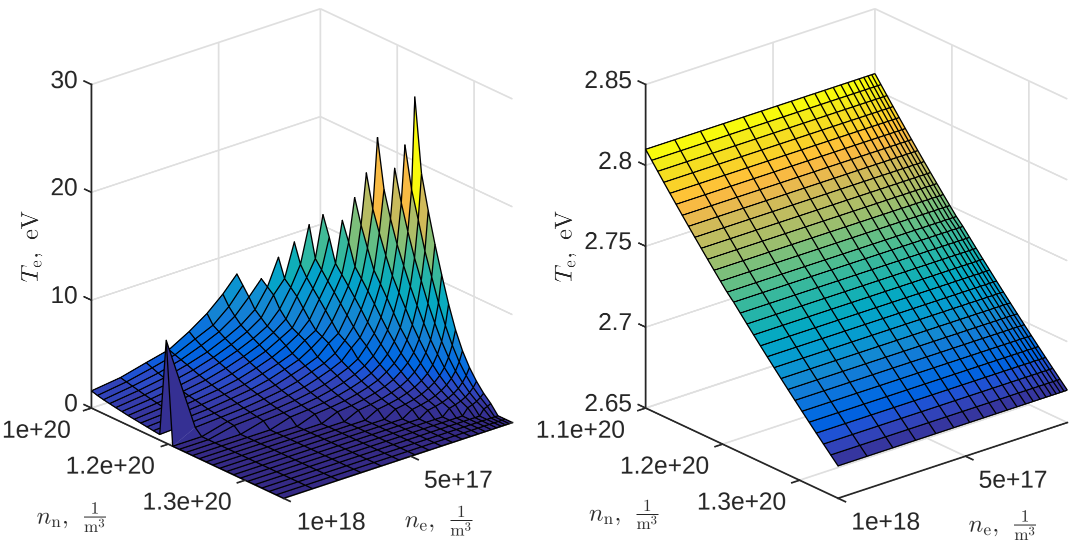

a) solution for mass conservation

b) solution for charge conservation

Figure 4. solution surface

In first order accuracy, we can also formulate $I_{\mathrm{b}} \propto \sqrt{T_{\mathrm{e}}} \cdot n_{\mathrm{e}}$. If n_{n} is reduced, the value of $\dot{m}_{\mathrm{n,neutral}}$ will also decrease, which has to be compensated by an increase of I_{b}. At constant n_{e} this increase is achieved by a higher T_{e} as apparent in Fig. 4 a). If n_{n} is kept constant, I_{b} will not change. Therefore, the formula $I_{\mathrm{b}} \propto \sqrt{T_{\mathrm{e}}} \cdot n_{\mathrm{e}}$ leads to higher T_{e} with lower n_{e} as also apparent in the figure. The statements from Sect. I are consolidated by the discontinuity at the bottom left side of Fig. 4 a). This discontinuity emerges because the chosen algorithm yields a second valid solution surface for the given boundary conditions. The ambiguity resulting from the ion optics behaviour is described in more detail in the Appendix. Figure 4 b) shows how the electron temperature drops with higher n_{n}.
The equation $\Delta P = 0$ yields an additional surface. A self-consistent solution for the whole model is given for the set of state quantities, where the three solution surfaces intersect. An elegant method to find this solution could be the multidimensional Newton–Raphson method. This may be faster than other approaches used, but also compromises a few of the problems described in section I.

D. Proposed approach

We show that the three-dimensional problem can be reduced to a set of three one-dimensional problems. To accomplish this, we already chose an appropriate structure for the system of equations introduced in subsection B. Here, the state quantities n_{n}, T_{e}, and n_{e} are used to describe the system's state. If we had chosen different variables, such as the ionization degree and the pressure, additionally unwanted couplings would be present. Furthermore, the appropriate boundary variables for the Eqs. 1, 2 and 3 have to be chosen. An often used strategy is:

a) To use the thruster's input variable U_{DC} and $\dot{m}_{\mathrm{p,neutral}}$ to calculate the resulting beam current I_{b}. Hereby, the mass efficiency is given as solution of the model and the resonance frequency f may be calculated self consistently.

Instead, we propose:

b) To use $\dot{m}_{\mathrm{p,neutral}}$ and the beam current I_{b} as boundary variables. Hereby, the mass efficiency is virtually given as input variable. Furthermore the model will yield the resonance frequency f as boundary variable. The required input voltage U_{DC} will be calculated.

This approach allows us to evaluate the optimal resonance frequency. Furthermore, the unknown values for n_{n}, T_{e}, and n_{e} can be found by solving balance equations sequentially. The resulting flow chart is depicted

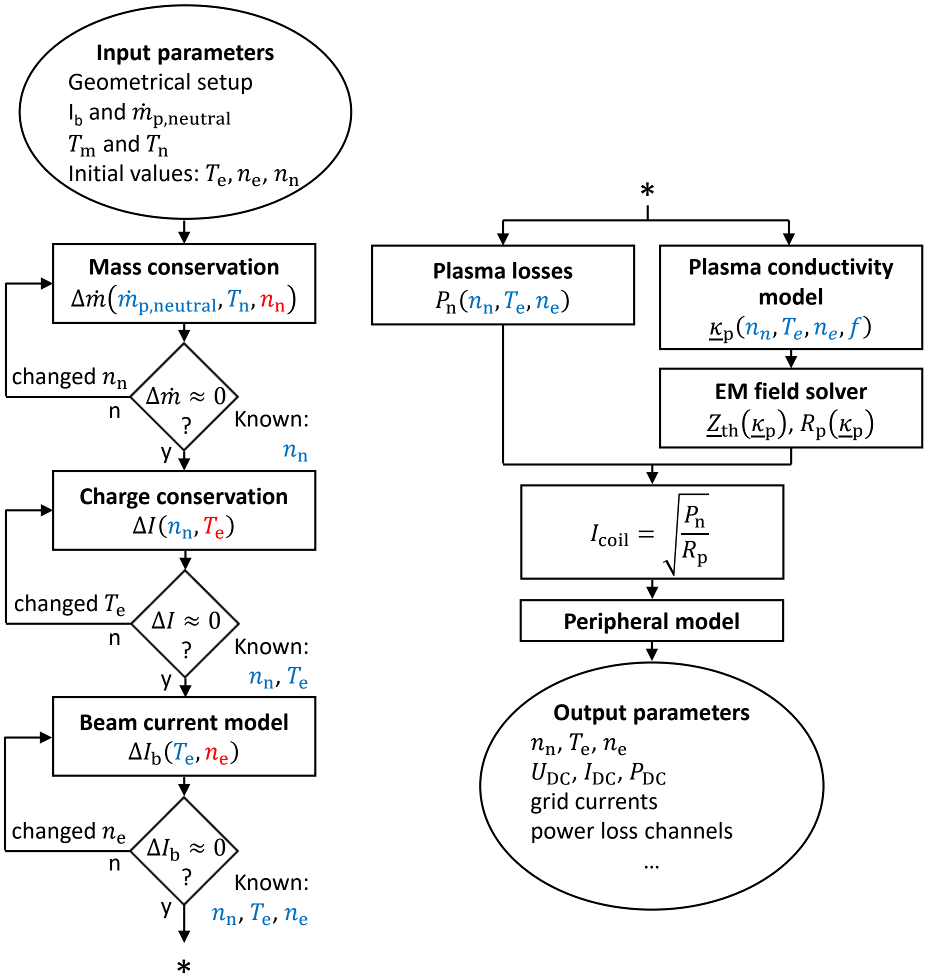

Figure 5. Proposed flow chart for solving the conservation laws

in Fig. 5. By using the beam current I_b as boundary condition $\dot{m}_{n,i}$ can be calculated directly. Therefore, the mass conservation with three unknown variable changes from

$$\Delta\dot{m}\left(\dot{m}_{p,neutral}, T_n, n_n, T_e, n_e\right) = \dot{m}_{p,neutral}\left(\right) - \dot{m}_{n,i}\left(T_e, n_e\right) + \dot{m}_{n,neutral}\left(T_n, n_n\right) = 0 \tag{6}$$

to

$$\Delta\dot{m}\left(\dot{m}_{p,neutral}, T_n, n_n\right) = \dot{m}_{p,neutral}\left(\right) - \dot{m}_{n,i}\left(\right) + \dot{m}_{n,neutral}\left(T_n, n_n\right) = 0 \tag{7}$$

with only one unknown variable by eliminating the dependence from the state quantities T_e and n_e. The remaining equation $\Delta\dot{m}\left(\dot{m}_{p,neutral}, T_n, n_n\right) = 0$ can be solved by an one-dimensional algorithm to search for zero crossings. This algorithm is depicted as a rhombus in Fig. 5. In our case we use a combination of the Newton's method, the regula falsi method, and a parabolic approximation of the searched function. In our model both I_p and I_n from the charge conservation formulated in Eq. 2 depend linearly on n_e. This is similar to other global models and allows us to eliminate this dependence on n_e.[8] Therefore, we can rewrite Eq. 2 as an one-dimensional problem with

$$\Delta I\left(n_n, T_e\right) = 0 \tag{8}$$

allowing us to derive T_e. As $\dot{m}_{n,i}\left(T_e, n_e\right)$ is proportional to I_b with a fixed factor we can describe $I_b\left(T_e, n_e\right)$ by the same dependence. This allows us to formulate the equation

$$\Delta I_b\left(T_e, n_e\right) = I_b\left(T_e, n_e\right) - I_{b,set} = 0 \tag{9}$$

where $I_{b,set}$ is the beam current set as boundary condition. This means we calculate n_e necessary to reach the required beam current for a given T_e. All state quantities are now known and $P_n\left(n_n, T_e, n_e\right)$ can be calculated directly. With the resonance frequency as boundary condition we can also calculate the plasma conductivity $\underline{\kappa}_{\mathrm{p}}(n_{\mathrm{n}}, n_{\mathrm{e}}, T_{\mathrm{e}}, f)$ which allows the EM field solver to derive the thruster's impedance $\underline{Z}_{\mathrm{th}}$ as well as the plasma resistance R_{p}. The coil current required to couple the power P_{n} into the plasma can be calculated using

$$I_{\mathrm{coil}} = \sqrt{\frac{P_{\mathrm{n}}}{R_{\mathrm{p}}}}. \tag{10}$$

The values for I_{coil} and $\underline{Z}_{\mathrm{th}}$ can be used as input variables for the peripheral simulation. Instead of a spice simulation as implied by Table 1 we utilize an analytical model for this purpose. Hereby, the resonance capacity is chosen to meet the resonance frequency set as boundary condition.

III. Results

In this chapter we will give a short example how the proposed approach can be used. By applying the sequential process each submodel can to some degree be examined individually to investigate its influence on the system's performance. This allows us to optimize the whole system by starting at the end of the proposed sequence of Fig. 5. For instance the input variables of the peripheral simulation can be used to generate an efficiency matrix as depicted on the left hand side of Fig. 6. The electrical efficiency of the

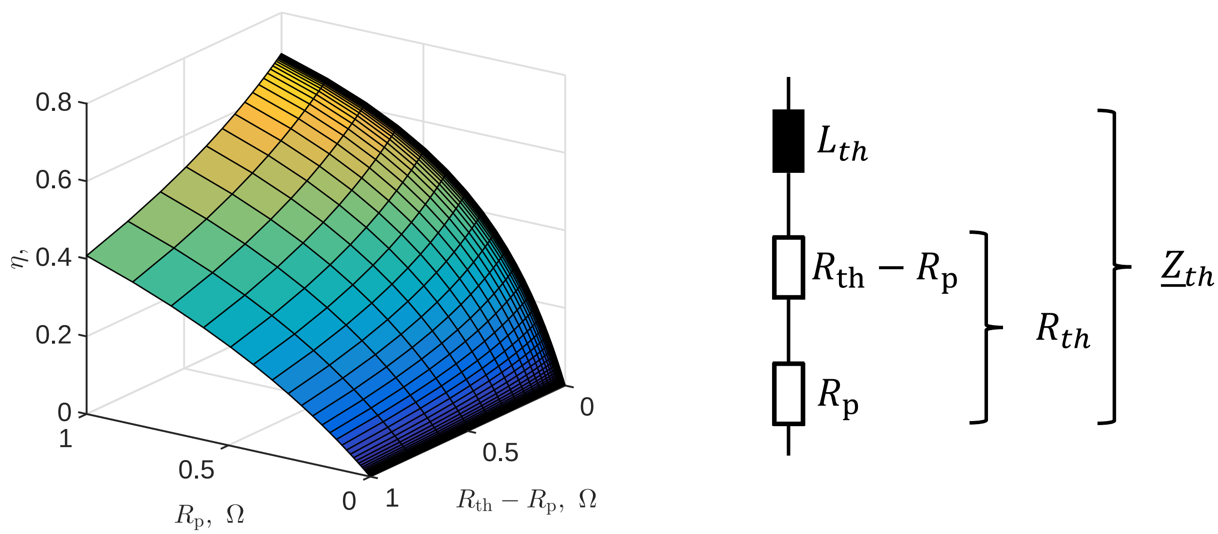

Figure 6. left: electrical efficiency of the peripheral system; right: thruster impedance

whole system is shown in dependence on the plasma resistance R_{p} and on the value of $R_{\mathrm{th}} - R_{\mathrm{p}}$. The latter value describes the losses which are not induced into the plasma, i.e. losses due to the current flowing in the coil as well as losses due to eddy currents in the housing etc. The right hand side of Fig 6 gives an overview how the thruster impedance is defined. The efficiency matrix is generated for a thruster inductance of 1.34 µH and plasma losses of $P_{\mathrm{p}} = 9.72$ W. With the given efficiency matrix the whole system can be optimized independently of remaining submodels by utilization of the EM field solver only. For instance, geometry studies could be made, which generate the values for R_{p} and $R_{\mathrm{th}} - R_{\mathrm{p}}$. Utilization of the efficiency matrix enables us to evaluate, whether the whole system's efficiency increases or decreases. Furthermore, an additional matrix can be generated which describes the influence of the EM field solvers output variables R_{p} and $R_{\mathrm{th}} - R_{\mathrm{p}}$ on its input variables, i.e. the plasma conductivity. This would allow us to evaluate how the plasma conductivity has to be influenced to get a higher electrical efficiency. For instance this can be done by choosing a different resonance frequency. In principle such matrixes can be generated for every submodel by investigating how the output variables change over the input variables.

IV. Conclusion

To simulate the RIT a complex system consisting of multiple coupled submodels is necessary and often utilized. The complexity of the model as well as the non-linear and non-monotonic behaviour of incorporated submodels complicate finding the self-consistent solution. The proposed scheme simplifies a three-dimensinal problem to a sequence of three 1D problems. It also reduces the amount of necessary iterations and therefore decreases the simulation time and the computational power respectively. The proposed structure also allows, one to estimate the influence of a single submodul on the system's performance. This can be used to clarify how certain parameters have to be set in order to optimize the system's performance.

Appendix

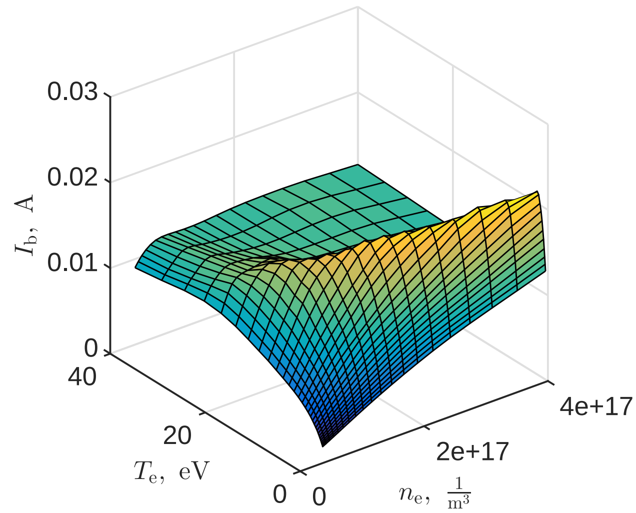

Figure 7. Beam current over T_e and n_e

If non-linear effects of the ion optics such as direct impingment and overcrossing are not considered the following correlation can be formulated for the beam current: $I_b \propto \sqrt{T_e} \cdot n_e$. This function behaves monotonic. A specific I_b corresponds to a unique set of values for T_e and n_e.
By simulating the ion optics the non-linear ion transmission coefficient is considered. This gives us the correlation: $I_b \propto \sqrt{T_e} \cdot n_e \cdot \tau_{i(T_e,n_e)}$, where the ion transmission coefficient τ_i depends on T_e and n_e. The result is depicted in Fig. 7 where the beam current is shown as a function of T_e and n_e. For the region shown in Fig. 7 where the values of both variables are small τ_i remains approximately constant. Accordingly, the beam current I_b scales with $\sqrt{T_e} \cdot n_e$. For higher values of T_e and n_e the ion transmission coefficient changes dramatically which influences the behaviour of the function. Subsequently, points of operation exist where the beam current will decrease, if T_e or n_e rise. For one value of n_e multiple values for T_e can exist with the same beam current.
The ambiguity in the left side of Fig. 4 is a result of this behaviour, i.e., for a fixed n_e a specific I_b corresponds to two values of T_e. Depending on the initial parameters of the algorithm used one or the other solution is found.

References

[1]H. Leiter, J. Kuhmann, R. Kukies, and J. P. Porst, "Results from the RIT-22 Technology Maturity Demonstration Activity ", *Proceedings of the* 50$^{\text{th}}$ *AIAA/ASME/SAE/ASEE Joint Propulsion Conference*, Cleveland, Ohio, 2014, Proceeding AIAA 2014-3421

[2]C. Volkmar, and U. Ricklefs, Eur. Phys. J. D **69**, No. 10 (2015), p. 227

[3]M. Dobkevicius, and D. Feili, Eur. Phys. J. D **70**, No. 11 (2016), p. 227

[4]M. Dobkevicius, and D. Feili, J. Propul. Power **33**, No. 4 (2017), p. 940

[5]C. Volkmar et al., "Real-time in situ determination of inductively coupled power and numerical prediction of power distribution in RF ion thrusters", *Proceedings of the 35th International Electric Propulsion Conference*, Atlanta, Georgia, 2017, Proceeding IEPC-2017-161

[6]A. Reeh, U. Probst, P. J. Klar, "3D Ion Extraction Code incorporated self-consistently into a numerical Model of a Radio-Frequency Ion Thruster", *Proceedings of the 35th International Electric Propulsion Conference*, Atlanta, Georgia, 2017, Proceeding IEPC-2017-326

[7]C. Volkmar, C. Geile, and K. Hannemann, J. Propul. Power **34**, No. 4 (2018), p. 1061

[8]A. Lieberman, and M. Lichtenberg, *Principles of Plasma Discharges and Materials Processing, Second Edition* (John Wiley & Sons, Hoboken, New Jersey, 2005)